AIP Physics of Fluids

Pinning of reaction fronts by burning invariant manifolds in extended flows

P. W. Megson, M. L. Najarian, K. E. Lilienthal, and T. H. Solomon

Citation: Physics of Fluids (1994-present) **27**, 023601 (2015); doi: 10.1063/1.4913380
View online: http://dx.doi.org/10.1063/1.4913380
View Table of Contents: http://scitation.aip.org/content/aip/journal/pof2/27/2?ver=pdfcov
Published by the AIP Publishing

PHYSICS OF FLUIDS 27, 023601 (2015)

Pinning of reaction fronts by burning invariant manifolds in extended flows

P. W. Megson,[a] M. L. Najarian,[b] K. E. Lilienthal,[c] and T. H. Solomon[d]
Department of Physics and Astronomy, Bucknell University, Lewisburg, Pennsylvania 17837, USA

(Received 12 October 2014; accepted 31 January 2015; published online 24 February 2015)

We present experiments on the behavior of reaction fronts in extended, vortex-dominated flows in the presence of an imposed wind. We use the ferroin-catalyzed, excitable Belousov-Zhabotinsky chemical reaction, which produces pulse-like reaction fronts. Two time-independent flows are studied: an ordered (square) array of vortices and a spatially disordered flow. The flows are generated with a magnetohydrodynamic forcing technique, with a pattern of magnets underneath the fluid cell. The magnets are mounted on a translation stage which moves with a constant speed V_d under the fluid, resulting in motion of the vortices within the flow. In a reference frame moving with magnets, the flow is equivalent to one with stationary vortices and a uniform wind with speed $W = V_d$. For a wide range of wind speeds, reaction fronts pin to the vortices (in a co-moving reference frame), propagating neither forward against the wind nor being blown backward. We analyze this pinning phenomenon and the resulting front shapes using a burning invariant manifold (BIM) formalism. The BIMs are one-way barriers to reaction fronts in the advection-reaction-diffusion process. Pinning occurs when several BIMs overlap to form a complete barrier that spans the width of the system. In that case, the shape of the front is determined by the shape of the BIMs. For the ordered array flow, we predict the locations of the BIMs numerically using a simplified model of the velocity field for the ordered vortex array and compare the BIM shapes to the pinned reaction fronts. We also explore transient behavior of the fronts (before reaching their steady state) to highlight the one-way nature of the BIMs. [http://dx.doi.org/10.1063/1.4913380]

I. INTRODUCTION

Many reacting systems are characterized by the propagation of a front that separates one species of the reaction from another. The front dynamics are affected dramatically by the presence of a fluid flow in the system. Front propagation in *advection-reaction-diffusion* (ARD) systems with fluid flows plays a critical role in such diverse systems as forest fires,[1] microfluidic chemical reactors,[2] plankton blooms in oceanic-scale flows,[3–5] ignition processes in Type-IA supernova explosions,[6,7] tumor growth,[8] and the spreading of a disease in a moving population.

There have been several recent studies of front propagation in laminar fluid flows. (See Tel *et al.*[9] for an overview of this subject up until 2005.) For time-independent, cellular flows,[10–14] reaction fronts are advected around vortices and burn across separatrices that block passive transport. For flows with periodic time-dependence, reaction fronts often mode-lock to the external

[a]Current address: Department of Physics, University of Maryland, College Park, Maryland 20742, USA. Electronic mail: pmegson@umd.edu
[b]Email: maya@bridj.com
[c]Email: kel014@bucknell.edu
[d]Email: tsolomon@bucknell.edu

forcing,[12,15,16] propagating an integer number of unit cells of the flow in an integer number of drive periods. There have also been experimental observations of pinning of reaction fronts in a chain of vortices with an imposed wind,[17] with the leading edge of pinned reaction fronts propagating neither forward against the wind nor backward with the wind relative to the vortices in the flow.

In this paper, we explore the pinning of reaction fronts in an extended, time independent flow composed of an ordered or disordered pattern of vortices with an imposed wind. We analyze this pinning behavior with a recent theory of *burning invariant manifolds* (BIMs).[18–20] These BIMs are extensions of invariant manifolds that act as barriers to passive transport. Unlike passive invariant manifolds, though, BIMs act as one-way barriers, blocking reaction fronts propagating in one direction while passing fronts that propagate in the opposite direction. We argue—through a combination of experimental studies and numerical BIM calculations—that the pinning is due to a combination of overlapping BIMs that together span the system and block the forward movement of the reaction front against the wind. The shape of pinned fronts is determined predominately by the pattern of BIMs which block the propagating fronts. We also explore transient front evolution as a mechanism to illustrate the influence of BIMs that are not revealed in the long-term, steady-state pinned fronts.

The experimental flow is time independent throughout this paper, either an ordered array of vortices or a spatially disordered, vortex-dominated flow. The fronts are produced by the ferroin-catalyzed Belousov-Zhabotinsky (BZ) chemical reaction. The BZ reaction has been used for a few decades as a paradigm for reaction-diffusion systems (with no flows);[21–23] consequently, it is a good system for studies of advection-reaction-diffusion processes.

In Sec. II, we present a background about burning invariant manifolds, discussing, in particular, how they can be calculated from a given velocity field. In Sec. III, we describe the experimental techniques used to generate the fluid flows, along with the details about the BZ reaction. Section IV shows experimental results showing the steady-state pinned fronts, along with transient behavior that elucidates the more detailed BIM structure for the ordered vortex array flow. The shapes of the pinned fronts for the ordered vortex array are compared with BIM patterns calculated numerically from a model of the flow, and some examples of pinned fronts are shown for the disordered flow. Section V discusses possible extensions of BIM approaches to more complicated flows, other systems that show pinning behavior, and continuing work.

II. BACKGROUND—BURNING INVARIANT MANIFOLDS

The mixing of passive impurities in time-independent and weakly time-dependent flows is strongly influenced by the presence of invariant manifolds in the flow that are attached to fixed points of the Eulerian velocity field[24,25] (Fig. 1(a)). (See discussion in Sec. V about extensions to more strongly time-dependent flows.) Passive invariant manifolds are absolute barriers to transport in the flow; in the absence of molecular diffusion, passive impurities will never cross an invariant manifold. The behavior is modified if there is a front-producing reaction occurring in the flow (Fig. 1(b)). A reaction triggered at an Eulerian fixed point will propagate out from that fixed point. Of course, there will be front movement along the unstable invariant manifold. But there will be outward propagation along the direction of the *stable* passive invariant manifold as well since the fluid velocity approaches zero at the Eulerian fixed point, whereas the front has an inherent propagation speed V_0 relative to the surrounding fluid. That outward propagation stops at *burning fixed points* (open circles) where the outward burning speed is balanced by the inward fluid velocity along the stable manifold.

Burning fixed points differ from Eulerian fixed points in an important respect: a burning fixed point has a direction associated with it. The left burning fixed point in Fig. 1(b), for instance, is a fixed point for left-propagating reaction fronts, whereas a front propagating to the right would pass through the same burning fixed point.

Each burning fixed point has associated BIMs. Unstable BIMs are shown in Fig. 1(b) for the two burning fixed points in the sketch. These BIMs act as barriers to front propagation, similar to invariant manifolds for passive transport. However, similar to the burning fixed points, BIMs have an associated direction. In Fig. 1(b), the left BIM blocks left-propagating reaction fronts and the

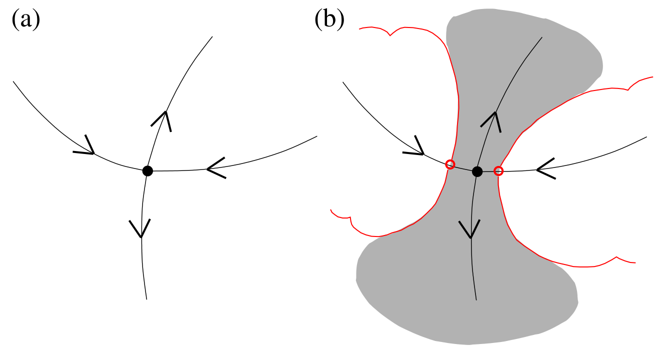

FIG. 1. (a) Cartoon of an Eulerian fixed point (filled dot) for a time-independent flow, along with stable and unstable passive invariant manifolds, indicated by inward- and outward-pointing arrows, respectively. (b) Spreading reaction (shaded) triggered at the Eulerian fixed point. The reaction expands most rapidly along the direction of the unstable passive invariant manifold, but it also burns outward in the stable direction, stopping at "burning fixed points" (open circles) on either side of the Eulerian fixed point. Attached to these burning fixed points are burning invariant manifolds which act as one-way barriers to front propagation. Both (a) and (b) are viewed from a reference frame where the flow is stationary.

right BIM blocks right-propagating fronts. If a reaction front is triggered to the left of both BIMs, it will propagate through the left BIM and converge on the right BIM. A reaction triggered to the right of both BIMs will pass through the right BIM and converge on the left.[18,19] A reaction triggered *between* the BIMs (e.g., at the Eulerian fixed point, as in Fig. 1(b)) will be blocked in both directions by the BIMs.

Mathematically, propagating reaction fronts can be described with a three-dimensional (3D) set of ordinary differential equations (ODEs) for an infinitesimal element of the front,[18]

$$\dot{x} = u_x + v_0 \sin\theta, \quad \dot{y} = u_y - v_0 \cos\theta, \tag{1a}$$

$$\dot{\theta} = -(u_{x,x} + u_{y,y}) \sin\theta \cos\theta - u_{x,y} \sin^2\theta + u_{y,x} \cos^2\theta, \tag{1b}$$

where dots denote time-derivatives. In these equations, distances x and y are scaled by the vortex width D (half of a unit cell of the flow), velocities are scaled by the maximum flow speed U measured along the separatrix between adjacent vortices in the absence of a wind, and time is scaled by the typical advective time scale D/U. Similar to the equations describing the trajectory of a passive tracer, there are two equations (Eq. (1a)) for the x- and y-motion of a front element, with the motion determined by a combination of the x- and y-velocities of flow (u_x and u_y, respectively) and front propagation at a non-dimensional speed $v_0 \equiv V_0/U$ relative to the surrounding fluid in a direction perpendicular to the front. But a front element has an angle θ relative to the positive x-axis, and there is third equation (Eq. (1b)) for θ to account for rotation of the front due to swirling of the flow. The model neglects small variations in v_0 due to curvature of the fronts.[26]

With this framework, the evolution of a front element is a trajectory in a three-dimensional phase space. The burning fixed points and BIMs seen in Fig. 1(b) are two-dimensional projections of these three-dimensional (x, y, θ) structures in (x,y)-space. Occasionally, these two-dimensional (2D) projections show a cusp—these cusps signify a change in the blocking direction for the BIM. Consequently, a reaction front wrapping around a BIM can pass through the BIM after the cusp.

Since burning fixed points reside in a 3D phase space, there are three directions of stability, unlike the Eulerian fixed points which have two.[20] The Eulerian fixed point (where fluid velocity is zero) in Fig. 1 in a 2D, (x,y) phase space is stable in one direction and unstable in the other (SU). The burning fixed points in Fig. 1(b) to the left and right of the Eulerian fixed point are stable in two directions and unstable in one (SSU). There are, however, two additional burning fixed points associated with this Eulerian fixed point, one above and one below (not shown in Fig. 1(b)). These fixed points correspond to front elements burning *toward* the Eulerian fixed point, since the fluid velocity is aimed away from the Eulerian fixed point along the unstable manifolds. (Note that burning fixed points need not lie exactly on the passive invariant manifolds.) These burning fixed points are stable in only one direction and unstable in the other two (SUU). BIMs attached to both

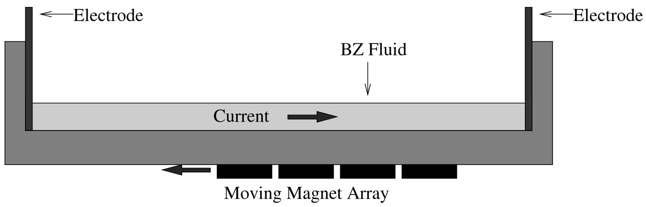

FIG. 2. Side view of experimental apparatus. A magnet assembly translates with constant velocity underneath a box containing a 2.7 mm layer of fluid that comprises the Belousov-Zhabotinsky reaction. An electrical current passing through this fluid layer interacts with the magnetic field to produce the flow.

SSU and SUU burning fixed points act as one-way barriers to front propagation. Due to the extra stable direction, BIMs attached to SSU burning fixed points are attracting for front trajectories in the 3D, (x, y, θ) space; in the 2D, (x, y) projections, BIMs attached to SSU burning fixed points are attracting for fronts approaching in the blocking direction (fronts going the other way pass through). On the other hand, BIMs attached to SUU burning fixed points are repelling for all fronts since there are two unstable directions. Consequently, the SSU (and not SUU) burning fixed points and their BIMs are the ones that we would most expect to see controlling the front patterns that we observe in the experiments.

We can calculate BIMs from Eqs. (1), given a velocity field (u_x, u_y) describing the flow. We identify a burning fixed point in the 3D ODEs by solving for x, y, and θ in Eqs. (1) where $\dot{x}$, $\dot{y}$, and $\dot{\theta}$ are all zero. We initialize a phase space trajectory very close to the burning fixed point. Integration of Eqs. (1) (using a 4th-order, Runge Kutta algorithm) results in a trajectory that closely approximates a branch of the unstable BIM for that burning fixed point.

III. EXPERIMENTAL TECHNIQUES

A. Flow

The flow is generated using a magnetohydrodynamic forcing technique (Fig. 2). An acrylic box (28 cm $\times$ 28 cm interior dimensions) with a thin layer of an electrolytic solution contains two stainless steel or brass electrodes on either side. An electrical current passing through the fluid interacts with a magnetic field produced by a pattern of Nd-Fe-Bo magnets below the box. Two arrangements of magnets are used: (a) an ordered, square array of 1.9 cm diameter magnets and (b) a spatially disordered pattern of 0.64 cm diameter magnets. The forcing results in either an ordered array of vortices (Fig. 3) or spatially disordered flow (Fig. 4).

The magnet assembly is mounted on a translation stage below the acrylic box. During an experimental run, the magnets translate with a constant velocity V_d below the box, resulting in translation of the vortices in the flow. In a reference frame moving with the translating magnets, the flow can be considered to be a stationary pattern of vortices (ordered or disordered) with a uniform imposed wind $W = V_d$. We define a non-dimensional wind speed $w = W/U$.

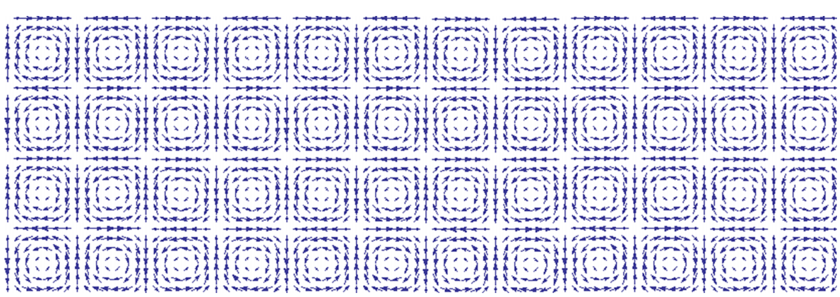

FIG. 3. Sketch of velocity field for ordered vortex array in the absence of an imposed wind.

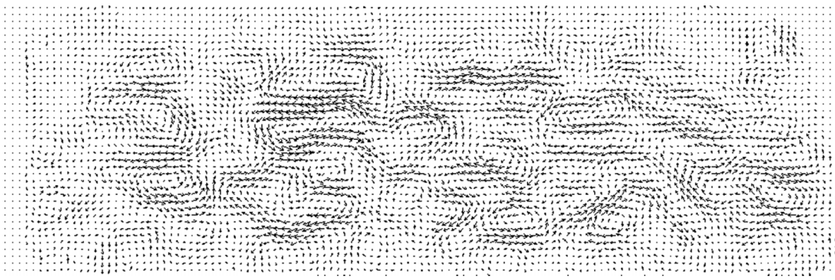

FIG. 4. Experimentally determined velocity field for the disordered flow, in the absence of an imposed wind. The field was determined by tracking tracer particles on the surface of the fluid.

The velocity field in the absence of an imposed wind can be determined approximately by tracking tracers floating on the surface of the fluid.[19] However, there are several limitations in the usefulness of the velocity field determined this way. First, there are serious questions about how faithfully buoyant particles on the surface track the fluid velocity in the flow. Second, the sampling of the velocity field is very non-uniform as tracers often miss closed regions in the flow either due to initial placement or due to centrifugal effects. Third, interpolation of the velocity field onto a uniform grid is problematic, especially in regions where the fluid velocity is weakest. Unfortunately, these weak-flow regions are often the most important as these are where the Eulerian fixed points are and where the burning fixed points are near. Consequently, the BIMs calculated from experimentally measured velocity fields can be inaccurate in the most important regions where the flow velocities are smallest. This is particularly tricky for experiments with the spatially disordered flow, for which the BIMs form an almost spaghetti-bowl pattern that can be difficult to discern, even if calculated accurately.

Consequently, we concentrate primarily on the studies with the ordered vortex array, since we have an analytical expression that reasonably approximates the velocity field[27]

$$\begin{aligned} du_x/dt = u_x(x,y,t) &= \sin(\pi x)\cos(\pi y), \\ du_y/dt = u_y(x,y,t) &= -\cos(\pi x)\sin(\pi y) - w. \end{aligned} \tag{2}$$

As before, velocities are non-dimensionalized by the maximum vortex speed U in the absence of an imposed wind, and distances are normalized by a vortex width (half the length of a unit cell of the flow).

This model (with $w = 0$) has been used successfully in several previous studies both of chaotic mixing and front propagation in a linear chain of vortices.[12,15,16,18,19,28,29] We note, however, that there are 3D components to the experimental flow, first because of the no-slip boundary condition at the bottom of the fluid layer, and also because of a weak, secondary, 3D flow due to Ekmann pumping[30] that circulates fluid up through the centers of vortices in the flow.

B. Belousov-Zhabotinsky reaction

The fronts in these experiments are produced by the excitable, ferroin-catalyzed, BZ chemical reaction.[22,31] A solution composed of 0.22 M sulfuric acid, 0.36 M sodium bromate, 0.12 M Malonic acid, and 0.12 M sodium bromide is mixed under a vent hood until clear. Ferroin indicator (0.025 M) is then added to turn the solution a deep orange color. (More ferroin is added periodically over the course of the experiments as the color fades.) The entire solution is poured into the apparatus, resulting in a 2.7 mm thick layer across the box.

After a sufficient amount of time (approximately an hour), bubbles from the initial reaction are swept away, and the fluid is stirred to wipe out any fronts that have self-triggered. A controlled front is then triggered by inserting a silver wire into the fluid. This wire oxidizes the indicator in the vicinity, changing the color of the fluid in that region from orange to blue-green. This region then oxidizes the surrounding fluid and so on, resulting in a front that propagates outward from the trigger point. (A line front can be triggered by drawing a line in the fluid with the silver wire.) In the

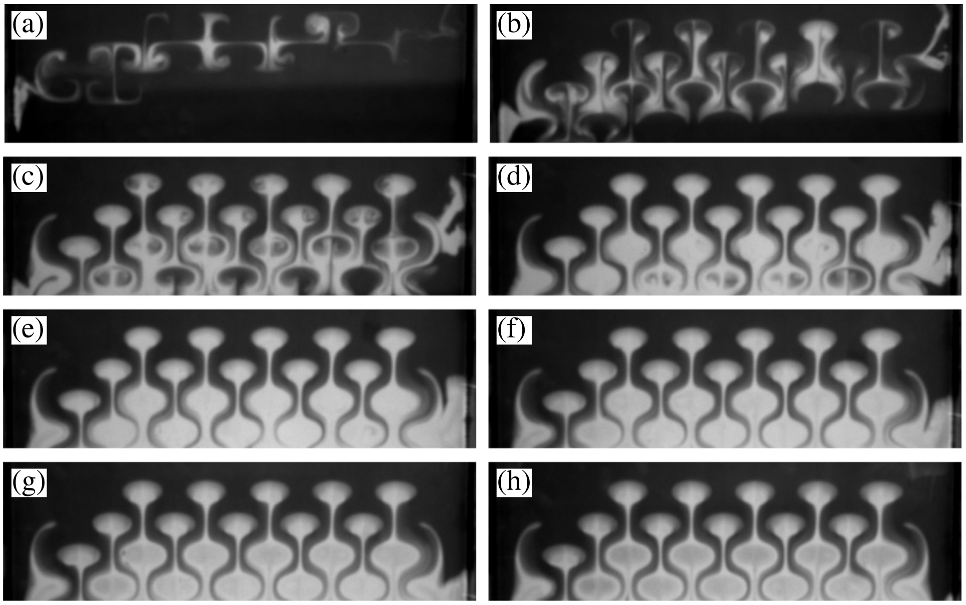

FIG. 5. Sequence of front images for regular vortex array, showing pinning behavior; $v_0 = 0.051$, $w = 0.52$. The full width (28 cm) of the apparatus is shown. These images are obtained from a reference frame in which the vortices are stationary, with a uniform wind blowing toward the bottom of the images. The images are separated in time by 25 s each.

absence of a fluid flow, the BZ fronts in these experiments propagate with a speed V_0 = 0.007 cm/s. The front is pulse-like—the region behind the front relaxes back to its original orange color, after which it can be re-triggered. In many cases, circulation in the flow returns part of the leading edge of the front to relaxed regions farther back, re-triggering a front automatically.

IV. RESULTS

A. Ordered vortex array

Previous experiments[32] explored the behavior of reaction fronts in a steady and oscillatory vortex array. For a stationary flow with no wind, a reaction front moves from vortex to vortex but overall propagates outward in coarse-grained, roughly circular pattern. The addition of a wind (in a reference frame moving with the magnet array, as discussed in Sec. III A) changes the behavior quite dramatically. For a wide range of wind speeds,[17] the leading edge of the front pins to the vortices. Figure 5 shows a sequence of images showing a reaction front that is triggered initially along a horizontal line. In a reference frame moving with the vortices (with a downward-directed wind), the front rapidly converges to a pinned state which remains unchanged (except for small variations at the edges) for the duration of the experiment, propagating neither forward against the wind nor being blown backward. In the lab frame (not shown in Fig. 5), after the initial transient, the reaction front translates along with the vortices without changing its shape.

The shape of the pinned front depends critically on the non-dimensional front and wind speed v_0 and w. Figure 6 shows steady reaction fronts for three different values of v_0. (In these experiments, v_0 is varied by changing the characteristic flow and wind velocities U and W, rather than by changing the reaction-diffusion front propagation speed V_0.) In particular, the front has significantly more detail for small v_0, whereas the front is smoother with less fine detail for larger v_0.

BIMs calculated from Eqs. (1) and (2) are shown in Figs. 6(d)-6(f). At the tops of each of the mushroom-shaped structures in these images, we display BIMs from two burning fixed points, one above and one below the Eulerian fixed point at the top of the mushroom. These Eulerian fixed points are the hyperbolic fixed points sketched in Fig. 3. Each of the BIMs is displayed up to the location of the first direction-changing cusp.

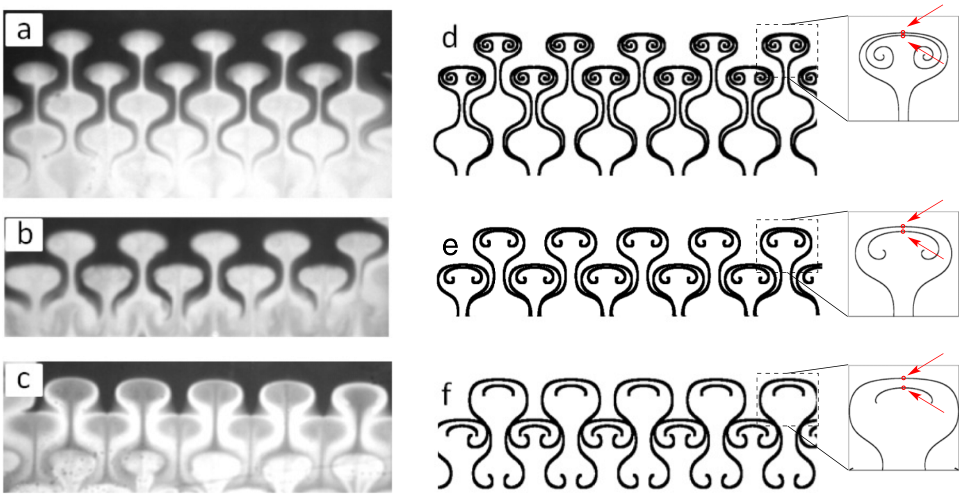

FIG. 6. Pinned reaction fronts in ordered vortex array flow, triggered initially along a horizontal line. A 20 cm wide sub-region of the flow is shown in all the images. (a)-(c) Experimental images of pinned BZ reaction fronts with (a) $v_0 = 0.051$, $w = 0.52$, (b) $v_0 = 0.099$, $w = 0.50$, (c) $v_0 = 0.19$, $w = 0.50$; (d)-(f) BIMs calculated theoretically from the velocity field given by Eq. (2); same parameters as (a)-(c). The zoomed-in panels on the right show the locations of the burning fixed points (dots, pointed to with arrows) for one of BIM structures. The Eulerian fixed points (not shown) in each case are in between the two burning fixed points.

In other experiments on front propagation and BIMs,[18,19] the BIMs were local barriers, but fronts could continue propagating past them in three different ways: (a) if the BIM did not span the entire region of interest (e.g., if the BIM forms an inward spiral), in which case the front could go around the BIM; (b) if there was a direction-changing cusp in the BIM, as in the cartoon in Fig. 1(b), in which case the front could pass through the BIM after the cusp; or (c) if the flow is time-dependent, the front could follow a continually stretching and undulating BIM across the flow, similar to how passive impurities can follow passive invariant manifolds with ever-increasing length and folded structure.

The BIM formalism explains why there is pinning of the fronts in the presence of an imposed wind. Pinning is possible for time-independent flows if either (a) a single BIM spans the entire system with no direction-changing cusps (which is not the case in these experiments) or (b) multiple BIMs with the same blocking direction overlap to produce a barrier that spans the entire system. It is this second mechanism that is the cause of the pinning in these experiments, as seen in Fig. 6.

Given a sewn patchwork of BIMs that produces a barrier, we would expect a steady-state, pinned front to have a shape that reflects the underlying BIM structure. Overall, as can be seen in Fig. 6, the BIM structure predicted from the front element model and velocity field (Eqs. (1) and (2)) captures the basic shape of the steady-state pinned reaction fronts, consistent with the proposition that the pinning is caused by overlapping BIMs in these experiments. The agreement is good, despite the fact that the model flow does not include weak three-dimensionality in the flow in the experiments due to the non-slip boundary condition at the bottom of the fluid layer and to Ekman pumping[30] that carries fluid up through the vortex centers.

For smaller v_0 (Figs. 6(a) and 6(d)), the burning fixed points are closer to the Eulerian fixed point and are therefore closer to each other, as can be seen in the zoomed-in panels at the right of Fig. 6. Consequently, the BIMs around a common Eulerian fixed point (which are attached to the burning fixed points) are closer together for smaller v_0, as can also be seen in Fig. 6. The outer BIMs in Fig. 6(d) block front propagation upward; these BIMs overlap with their neighbors, resulting in a patchwork of overlapping upward-blocking BIMs that spans the system, allowing for a pinned front whose shape matches the pattern of overlapping BIMs. For the value of v_0 in Figs. 6(a) and 6(d), the BIMs do not overlap until they have penetrated back downwind by more than three vortices. Consequently, there are long, thin, unburned tendrils in the front pattern (Fig. 6(a)) between the burned (reacted) regions.

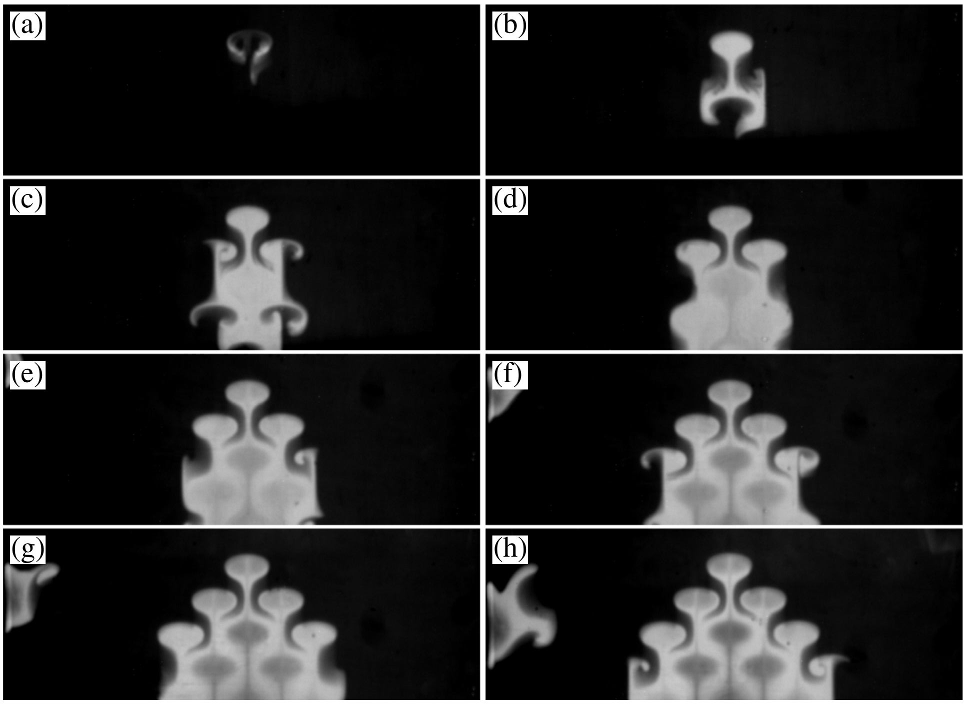

FIG. 7. Sequence of front images for regular vortex array, with an initial point trigger; $v_0 = 0.099$, $w = 0.050$. The full 28 cm width of the apparatus is shown. The images—separated in time by 50 s—are taken from a reference frame moving with the vortices, with a uniform wind directed toward the bottom of the page.

For larger v_0, the burning fixed points and the BIMs have a larger separation from the Eulerian fixed points, as seen by the BIMs near the tops of the mushrooms in Fig. 6(f) and in its zoomed-in panel. In this case, the BIMs from neighboring vortices overlap within one vortex distance downwind, resulting in a pinned reaction front with much smaller unburned tendrils and a significantly smoother overall shape (Fig. 6(c)).

Since there is an array of vortices in this flow, each with their own combination of BIMs, the pinned structures seen in Fig. 6 are not the only ones possible in this system. Depending on how the reaction front is initially triggered, the front can pin to different combinations of BIMs in the flow, allowing for a range of different pinned front shapes. As an example, Fig. 7 shows the evolution of a front triggered at a point rather than along a line. Instead of horizontal pinned structure (as in Fig. 6 with a horizontal line trigger), a staircase structure develops, with the leading edge rapidly converging to a pinned shape while the trailing portion is still developing. Figs. 6 and 7 are just two of many different pinned shapes that are possible in this flow.

There are some subtleties of the nature of the BIMs that cannot be elucidated with steady-state, pinned fronts. In particular, the one-way nature of these BIMs as barriers shows up much more readily by looking at the transient behavior of the reaction fronts. Figure 8 shows a sequence that elucidates the blocking behavior of both BIMs within a single mushroom structure. A reaction front propagating downward passes through the outer BIM (which blocks outward-moving fronts) but does not cross over the inner BIM (which blocks inward-moving fronts). Instead, the front winds around in the space between the two BIMs. Once inside the outer BIM, it is now trapped by that BIM as it traces out the left side of the mushroom shape. The reaction finally penetrates into the middle of the structure after reaching the end of the inward-blocking part of the inner BIM. (In Fig. 8, the inner BIM is displayed up to the point where there is a direction-changing cusp.)

The behavior of fronts near a BIM cusp can be seen in Fig. 9. A downward-propagating reaction front passes through the outer BIM (not shown in Fig. 9)—which blocks outward-propagating fronts—and is blocked by the top part of the inner BIM, which blocks inward-propagating fronts.

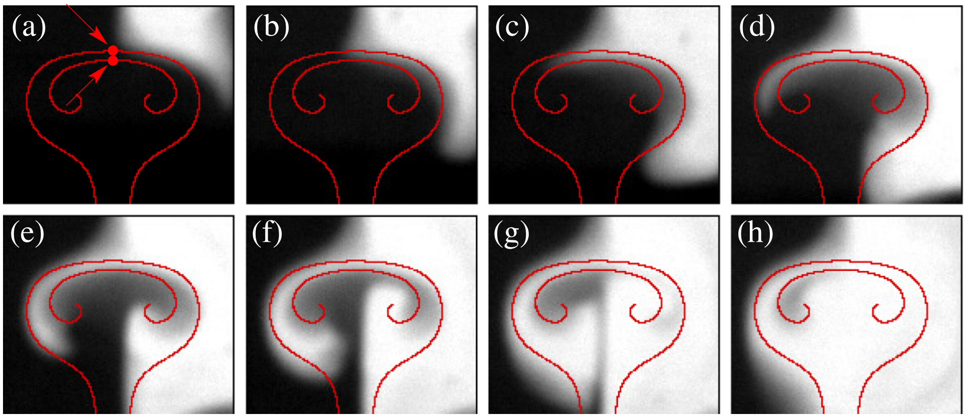

FIG. 8. Sequence of images showing the transient blocking by an interior BIM; $v_0 = 0.099$, $w = 0.50$; images are separated by 4.0 s each. The curves show an outward-blocking BIM (the outside one) and an inward-blocking BIM (the inside one). The dots and arrows in (a) denote the locations of two of the burning fixed points.

It moves around this BIM until it reaches the cusp, at which the BIM starts blocking outward-propagating fronts, and the front moves into the center.

B. Spatially disordered flow

Experiments with the spatially disordered flow (Fig. 4) proceed in the same way as those for the ordered vortex array, except that there is not an analytical expression that we can use to approximate the velocity field. As with the ordered vortex array flow, we impose a wind by translating the (disordered) magnet assembly underneath the fluid and transforming to a reference frame in which the magnets—and the disordered flow produced by them—are stationary.

As is the case with the ordered array, the presence of a wind causes fronts in the flow to pin to the underlying flow structure. Figure 10 shows several images of stationary fronts (as viewed in the co-moving reference frame) for different flow parameters. Figures 10(a)–10(c) show the pinned front for increasing wind strengths but with the same non-dimensional front propagation speed v_0. Figure 10(d) shows a pinned front for a non-dimensional wind close to that for Fig. 10(c), but with a significantly larger v_0. As is the case with pinned fronts for the ordered vortex array, the pinned front is smoother for larger v_0 (Fig. 10(d)). There are also clear variations in the pinning pattern with varying wind.

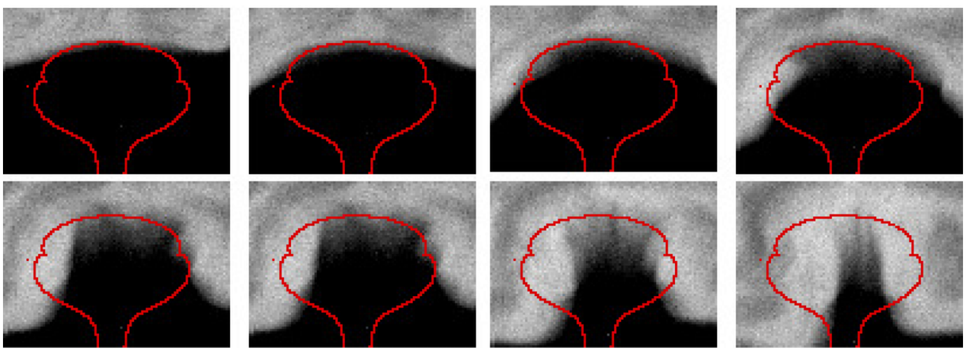

FIG. 9. Sequence showing direction-changing nature of cusps in BIMs; $v = 0.19$, $w = 0.50$. A front propagating downward is blocked by the top portion of the BIM which blocks inward-directed fronts. The blocking direction changes at the two cusps, and the front wraps around and penetrates into the middle after circumnavigating these cusps.

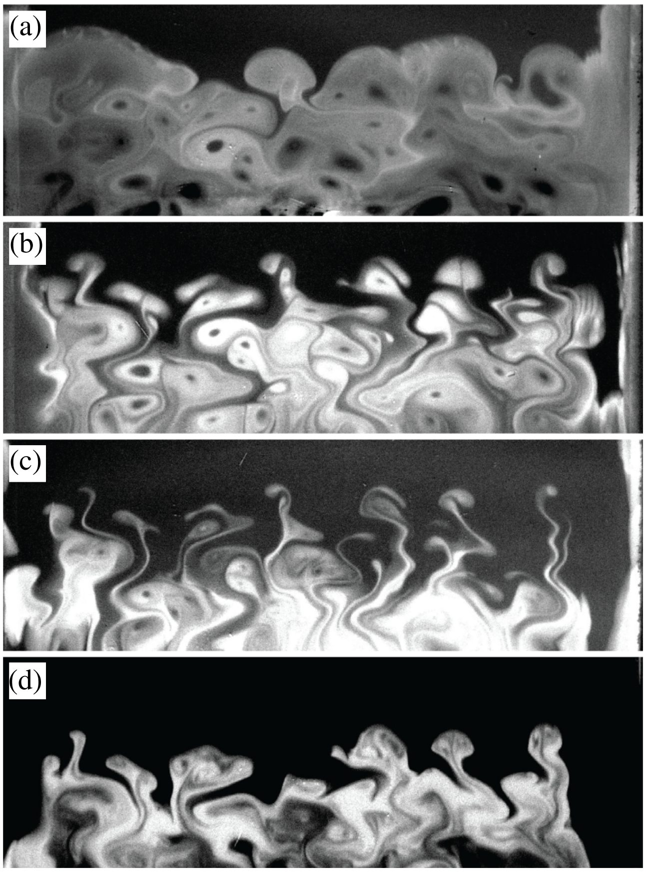

FIG. 10. Pinned reaction fronts for disordered velocity field with imposed wind (directed toward bottom of page). The full 28 cm width of the flow is shown. Non-dimensional front speed $v_0 = 0.016$ for (a)-(c) and 0.11 for (d). Non-dimensional wind speeds are 0.052, 0.21, 0.37, and 0.42 for (a)–(d), respectively.

As with the pinned fronts for the ordered array, we argue that the pinning is caused by a pattern of overlapping BIMs. (Note that calculating these BIMs from the experimental velocity field, although possible, is challenging due to a lack of precision in the measured velocity field—especially near the fixed points as viewed in the co-moving reference frame where the fluid speeds are smallest—and the complicated nature of the flow and the many BIMs.) The thinner structures—which are stationary despite their complexity—found for the larger winds (Fig. 10(c)) are due to BIMs that follow the wind downstream before broadening sufficiently to overlap. And the smoother structures for larger v_0 (Fig. 10(d)) are due to the larger separation of the BIMs for large v_0, resulting in BIMs that overlap without having to go too far downwind.

V. DISCUSSION

These experiments provide further evidence of the significant role played by barriers in front propagation and in fluid mixing, in general. The importance of barriers for passive fluid mixing has received significant attention recently in the context of *Lagrangian Coherent Structures*[33–35] which are sometimes referred to as the "skeleton" for understanding transport in flows with aperiodic time dependence. Similarly, we believe that a complete understanding of barriers to front propagation is critical for developing the skeleton of a larger theory of front propagation in fluid flows. And in conjunction with other recent experiments, these pinning results indicate that burning invariant manifolds may provide the theoretical background for characterizing barriers to front motion in fluid flows.

Characterizing and predicting persistent reaction structures are challenging for time-aperiodic and turbulent flows for which stable and unstable manifolds of fixed points cannot rigorously be defined. For passive mixing (no reaction) systems, several techniques have been proposed during the past few years to predict persistent mixing structures, including finite-time Lyapunov exponent (FTLE) fields,[33,35] hypergraph and mesohyperbolicity/mesoellipticity techniques,[36] variational approaches,[37] ergodic partition,[38] and finite-time curvature fields.[39] Alternately, there are techniques for defining invariant manifolds for chaotic sets for time-dependent flows.[40–42] These various techniques use the 2D equations of motion for a particle trajectory $dx/dt = u_x$ and $dy/dt = u_y$ for their analyses. We speculate that similar approaches using the 3D equations for front elements (Eqs. (1)) will ultimately be able to predict persistent structures for propagating reaction fronts in a range of time-aperiodic and turbulent flows.

The pinning seen in these flows is similar in many respects to pinning seen of chemical reaction fronts in a porous media with a through flow.[43,44] In those experiments and simulations, the tendency of fronts to remain stationary in the face of an imposed wind was explained with arguments based on heterogeneities in the system due to the porous media and, in particular, on the no-slip boundary conditions of the fluid flows near the grains in the porous media. As we have shown in the current experiments, though, it is not necessary to have fixed surfaces and no-slip boundary conditions to have pinned reaction fronts in an ordered or spatially disordered flow with a wind. Pinning of reaction fronts in a flow through a porous media can be explained by considering recirculation zones in the flow near and around the spheres in the porous media (see, e.g., Biemond *et al.*[45]).

We expect the pinning behavior seen in these experiments—along with the central importance of burning invariant manifolds in the process—to be a general result that applies to a range of front-producing systems in fluid flows. As an example, a 2004 study[3] of plankton blooms in oceanic flows found similar pinning phenomena, referred to as "persistent patterns" in that study. The BIM theory does not depend on the specific nature of the reaction—all that is needed is a velocity field and a front with a well-defined propagation speed V_0 in the absence of a flow.

Pinning and depinning phenomena extend to a wide range of condensed matter systems, including charge density waves[46,47] and vortex pinning in type-II superconductors.[48,49] There are also general theories of wave front depinning that employ reaction-diffusion modelling.[50] In the other pinning systems, there is typically some sort of heterogeneity in the system, similar in some respects to the heterogeneity introduced in these experiments by the vortices in the flow. And there is some sort of forcing with a critical depinning threshold, similar to the role played by the uniform wind in these experiments. As to whether there is an analogue of the burning invariant manifolds in those other pinning systems, that is an area for future research.

A more complete discussion of the theory and the mathematical background behind front pinning (using BIM analysis) are currently being written and will be published separately. We are also continuing our experimental studies of pinning of reaction fronts, looking at flows with periodic and aperiodic time dependence, as well as fully three-dimensional flows, for which a BIM theory of front elements will require a five-dimensional phase space (x, y, z, θ, ϕ), i.e., 3 spatial coordinates for the location of the front elements and 2 angles to denote the orientation of the front element.

ACKNOWLEDGMENTS

These studies were supported by the US National Science Foundation under Grant Nos. DMR-1004744, PHY-1156964, DUE-1317446, and DMR-1361881. We gratefully acknowledge numerous conversations with Kevin Mitchell and John Mahoney. We would also like to thank the assistance of Jack Raup and Moises Veloz in the construction of the apparatus for these experiments.

[1] W. Hargrove, R. H. Gardner, M. G. Turner, W. H. Romme, and D. G. Despain, "Simulating fire patterns in heterogeneous landscapes," Ecol. Modell. **135**, 243–263 (2000).
[2] T. John and I. Mezic, "Maximizing mixing and alignment of orientable particles for reaction enhancement," Phys. Fluids **19**, 123602 (2007).
[3] E. Hernandez-Garcia and C. Lopez, "Sustained plankton blooms under open chaotic flows," Ecol. Complexity **1**, 253–259 (2004).

[4] M. Sandulescu, C. Lopez, E. Hernandez-Garcia, and U. Feudel, "Biological activity in the wake of an island close to a coastal upwelling," Ecol. Complexity **5**, 228–237 (2008).
[5] D. Bastine and U. Feudel, "Inhomogeneous dominance patterns of competing phytoplankton groups in the wake of an island," Nonlinear Processes Geophys. **17**, 715–731 (2010).
[6] F. K. Ropke, W. Hillebrandt, and J. C. Niemeyer, "The cellular burning regime in type Ia supernova explosions," Astron. Astrophys. **421**, 783–795 (2004).
[7] C. M. Malone, A. Nonaka, S. E. Woosley, A. S. Almgren, J. B. Bell, S. Dong, and M. Zingale, "The deflagration stage of Chandrasekhar mass models for type Ia supernovae. I. Early evolution," Astrophys. J. **782**, 1–24 (2014).
[8] S. M. Wise, J. S. Lowengrub, H. B. Frieboes, and V. Cristini, "Three-dimensional multispecies nonlinear tumor growth – I. Model and numerical method," J. Theor. Biol. **253**, 524–543 (2008).
[9] T. Tel, A. de Moura, C. Grebogi, and G. Karolyi, "Chemical and biological activity in open flows: A dynamical system approach," Phys. Rep. **413**, 91–196 (2005).
[10] M. Abel, A. Celani, D. Vergni, and A. Vulpiani, "Front propagation in laminar flows," Phys. Rev. E **64**, 046307 (2001).
[11] M. Abel, M. Cencini, D. Vergni, and A. Vulpiani, "Front speed enhancement in cellular flows," Chaos **12**, 481 (2002).
[12] M. S. Paoletti and T. H. Solomon, "Front propagation and mode-locking in an advection-reaction-diffusion system," Phys. Rev. E **72**, 046204 (2005).
[13] A. Pocheau and F. Harambat, "Effective front propagation in steady cellular flows: A least time criterion," Phys. Rev. E **73**, 065304 (2006).
[14] A. Tzella and J. Vanneste, "Front propagation in cellular flows for fast reaction and small diffusivity," Phys. Rev. E **90**, 011001(R) (2014).
[15] M. Cencini, A. Torcini, D. Vergni, and A. Vulpiani, "Thin front propagation in steady and unsteady flows," Phys. Fluids **15**, 679 (2003).
[16] M. S. Paoletti and T. H. Solomon, "Experimental studies of front propagation and mode-locking in an advection-reaction-diffusion system," Europhys. Lett. **69**, 819 (2005).
[17] M. E. Schwartz and T. H. Solomon, "Chemical reaction fronts in ordered and disordered cellular flows with opposing winds," Phys. Rev. Lett. **100**, 028302 (2008).
[18] J. Mahoney, D. Bargteil, M. Kingsbury, K. Mitchell, and T. Solomon, "Invariant barriers to reactive front propagation in fluid flows," Europhys. Lett. **98**, 44005 (2012).
[19] D. Bargteil and T. Solomon, "Barriers to front propagation in ordered and disordered vortex flows," Chaos **22**, 094107 (2012).
[20] K. A. Mitchell and J. R. Mahoney, "Invariant manifolds and the geometry of front propagation in fluid flows," Chaos **22**, 037104 (2012).
[21] L. Kuhnert and H.-J. Krug, "Kinetics of chemical waves in the acidic bromate-malonic acid-tris(bipyridine)ruthenium(2+) system in comparison with the ferroin system," J. Phys. Chem. **91**, 730 (1987).
[22] S. K. Scott, *Oscillations, Waves, and Chaos in Chemical Kinetics* (Oxford University Press, Oxford, 1994).
[23] M. K. R. Reddy, Z. Nagy-Ungvarai, and S. C. Muller, "Effect of visible-light on wave-propagation in the ruthenium-ctalyzed Belousov-Zhabotinsky reaction," J. Phys. Chem. **98**, 12255 (1994).
[24] J. M. Ottino, *The Kinematics of Mixing: Stretching, Chaos and Transport* (Cambridge University Press, Cambridge, 1989).
[25] S. Wiggins, *Chaotic Transport in Dynamical Systems* (Springer-Verlag, New York, 1992).
[26] Z. Neufeld and E. Hernandez-Garcia, *Chemical and Biological Processes in Fluid Flows: A Dynamical Systems Approach* (Imperial College Press, 2009).
[27] S. Chandresekhar, *Hydrodynamic and Hydromagnetic Stability* (Clarendon, Oxford, 1961).
[28] T. H. Solomon and J. P. Gollub, "Chaotic particle transport in time-dependent Rayleigh-Bénard convection," Phys. Rev. A **38**, 6280 (1988).
[29] T. H. Solomon, S. Tomas, and J. L. Warner, "Role of lobes in chaotic mixing of miscible and immiscible impurities," Phys. Rev. Lett. **77**, 2682 (1996).
[30] T. H. Solomon and I. Mezić, "Uniform resonant chaotic mixing in fluid flows," Nature **425**, 376 (2003).
[31] R. J. Field and M. Burger, *Oscillations and Traveling Waves in Chemical Systems* (Wiley, New York, 1985).
[32] J. R. Boehmer and T. H. Solomon, "Fronts and trigger wave patterns in an array of oscillating vortices," Europhys. Lett. **83**, 58002 (2008).
[33] G. A. Voth, G. Haller, and J. P. Gollub, "Experimental measurements of stretching fields in fluid mixing," Phys. Rev. Lett. **88**, 254501 (2002).
[34] C. Coulliette, F. Lekien, J. D. Paduan, G. Haller, and J. E. Marsden, "Optimal pollution mitigation in Monterey Bay based on coastal radar data and nonlinear dynamics," Environ. Sci. Technol. **41**, 6562–6572 (2007).
[35] M. Mathur, G. Haller, T. Peacock, J. E. Ruppert-Felsot, and H. L. Swinney, "Uncovering the Lagrangian skeleton of turbulence," Phys. Rev. Lett. **98**, 144502 (2007).
[36] I. Mezic, S. Loire, V. A. Fonoberov, and P. Hogan, "A new mixing diagnostic and Gulf oil spill movement," Science **330**, 486–489 (2010).
[37] M. Farazmand and G. Haller, "Attracting and repelling Lagragian coherent structures from a single computation," Chaos **23**, 023101 (2013).
[38] M. Budisic and I. Mezic, "Geometry of the ergodic quotient reveals coherent structures in flows," Physica D **241**, 1255–1269 (2012).
[39] T. Ma and E. M. Bollt, "Shape coherence and finite-time curvature evolution," Int. J. Bifurcation Chaos (in press).
[40] J. Franaszek, "Periodically kicked Duffing oscillator and nonattracting chaotic sets," Phys. Rev. E **49**, 3927–3929 (1994).
[41] A. Péntek, T. Tél, and Z. Toroczkai, "Chaotic advection in the velocity field of leapfrogging vortex pairs," J. Phys. A: Math. Gen. **28**, 2191–2216 (1995).
[42] T. Tél and Y.-C. Lai, "Chaotic transients in spatially extended systems," Phys. Rep. **460**, 245–275 (2008).
[43] M. Kaern and M. Menzinger, "Propagation of excitation pulses and autocatalytic fronts in packed-bed reactors," J. Phys. Chem. B **106**, 3751–3758 (2002).

[44] S. Saha, S. Atis, D. Salin, and L. Talon, "Phase diagram of sustained wave fronts opposing the flow in disordered porous media," Europhys. Lett. **101**, 38003 (2013).
[45] J. B. Biemond, A. P. S. de Moura, G. Karolyi, C. Grebogi, and H. Nijmeijer, "Onset of chaotic advection in open flows," Phys. Rev. E **78**, 016317 (2008).
[46] *Charge Density Waves in Solids*, edited by L. P. Gor'kov and G. Gruner (North Holland, Amsterdam, 1989).
[47] E. Pinsolle, N. Kirova, V. L. R. Jacques, A. A. Sinchenko, and D. L. Bolloc'h, "Creep, flow and phase slippage regimes: An extensive view of the sliding charge-density wave revealed by coherent x-ray diffraction," Phys. Rev. Lett. **109**, 256402 (2012).
[48] D. R. Nelson and V. M. Vinokur, "Boson localization and correlated pinning of superconducting vortex array," Phys. Rev. B **48**, 13060–13097 (1993).
[49] M. Velez, J. I. Martin, J. E. Villegas, A. Hoffmann, E. M. Gonzalez, J. L. Vicent, and I. K. Schuller, "Superconducting vortex pinning with artificial magnetic nanostructures," J. Magn. Magn. Mater. **320**, 2547–2562 (2008).
[50] A. Carpio and L. L. Bonilla, "Wave front depinning transition in discrete one-dimensional reaction-diffusion systems," Phys. Rev. Lett. **86**, 6034–6037 (2001).